JOURNAL OF GEOPHYSICAL RESEARCH, VOL. 113, G04015, doi:10.1029/2008JG000718, 2008



# Interannual variability of photosynthesis across Africa and its attribution

Christopher A. Williams,[1] Niall P. Hanan,[2] Ian Baker,[3] G. James Collatz,[4] Joseph Berry,[5] and A. Scott Denning[3]

Received 25 February 2008; revised 18 June 2008; accepted 19 August 2008; published 6 November 2008.

[1] Africa is thought to be a large source of interannual variability in the global carbon cycle, only vaguely attributed to climate fluctuations. This study uses a biophysical model, Simple Biosphere, to examine in detail what specific factors, physiological (acute stress from low soil water, temperature, or low humidity) and biophysical (low vegetation radiation use), are responsible for spatiotemporal patterns of photosynthesis across the African continent during the period 1982–2003. Acute soil water stress emerges as the primary factor driving interannual variability of photosynthesis for most of Africa. Southern savannas and woodlands are a particular hot spot of interannual variability in photosynthesis, owing to high rainfall variability and photosynthetic potential but intermediate annual rainfall. Surprisingly low interannual variability of photosynthesis in much of the Sudano-Sahelian zone derives from relatively low vegetation cover, pronounced humidity stress, and somewhat lower rainfall variability, whereas perennially wet conditions diminish interannual variability in photosynthesis across much of the Congo Basin and coastal West Africa. Though not of focus here, the coefficient of variation in photosynthesis is notably high in drylands and desert margins (i.e., Sahel, Greater Horn, Namib, and Kalahari) having implications for supply of food and fiber. These findings emphasize that when considering impacts of climate change and land surface feedbacks to the atmosphere, it is important to recognize how vegetation, climate, and soil characteristics may conspire to filter or dampen ecosystem responses to hydroclimatic variability.

**Citation:** Williams, C. A., N. P. Hanan, I. Baker, G. J. Collatz, J. Berry, and A. S. Denning (2008), Interannual variability of photosynthesis across Africa and its attribution, *J. Geophys. Res.*, *113*, G04015, doi:10.1029/2008JG000718.

## 1. Introduction

[2] The rise of atmospheric carbon dioxide, its relation to global warming, and the imbalance between anthropogenic emissions and atmospheric growth rates have concentrated much research on understanding surface sources and sinks of $CO_2$ and the biosphere's ability to offset anthropogenic carbon emissions. The net source/sink strength of tropical lands is highly uncertain and continues to be a subject of controversy with recent indication that tropical lands may be absorbing more carbon than previously thought [*Baker*, 2007]. However, sizable climate-induced interannual variability in these regions [*Houghton*, 2000] makes estimates strongly sensitive to their temporal window. For example, much of Africa experiences multiyear drought cycles [e.g., *Charney*, 1975; *Nicholson*, 2000; *Nicholson and Entekhabi*, 1986; *Tyson et al.*, 2002], suggesting that a window shorter than multiple drought cycles may confer substantial bias relative to the true long-term mean or trend.

[3] Global-scale time-dependent inverse analyses of atmospheric $CO_2$ distributions that begin to address this concern indeed find a large fraction of interannual variability in global sources and sinks of $CO_2$ arising from tropical lands [*Baker et al.*, 2006; *Bousquet et al.*, 2000; *Rayner et al.*, 2005; *Rödenbeck et al.*, 2003]. Still, lack of data and transport errors limit their ability to resolve the complicated patterns of source/sink dynamics as they respond to weather and climate anomalies. Furthermore, the inverse approach offers little mechanistic understanding about underlying processes to which spatial and temporal patterns can be attributed, something that is currently informed primarily with biophysical, biogeochemical, and ecosystem "process" models.

[4] Process models similarly attribute a large fraction of global interannual variability (IAV) in net ecosystem exchange (*NEE*) to tropical lands largely driven by climate fluctuations [*McGuire et al.*, 2001; *Williams et al.*, 2007].

[1] Graduate School of Geography, Clark University, Worcester, Massachusetts, USA.
[2] Natural Resource Ecology Laboratory, Colorado State University, Fort Collins, Colorado, USA.
[3] Department of Atmospheric Sciences, Colorado State University, Fort Collins, Colorado, USA.
[4] Biospheric Sciences Branch, Hydrospheric and Biospheric Sciences Laboratory, NASA Goddard Space Flight Center, Greenbelt, Maryland, USA.
[5] Carnegie Institution for Science, Washington, D. C., USA.


0148-0227/08/2008JG000718$09.00

Africa, one of the least well-understood components of the global and tropical picture [*Williams et al.*, 2007], reportedly contributes up to ~30% of the year-to-year variation in global land net $CO_2$ source/sink dynamics [*McGuire et al.*, 2001]. Interannual variability in land carbon fluxes is dominated by physiology (photosynthesis and respiration) and fires. Africa leads all other continents in annual fire emissions but with relatively small interannual variability [*van der Werf et al.*, 2006]. Therefore the balance between photosynthesis and respiration is expected to be particularly important in governing Africa's interannual variability of *NEE*. Furthermore, photosynthesis plays a central role in *NEE* not only as the $CO_2$ uptake flux but also as it provides the substrate for the respiratory flux into the atmosphere.

[5] Model-derived estimates of global terrestrial photosynthesis are many [e.g., *Ciais et al.*, 2001]. However, few analyses investigate how bioclimate determines terrestrial photosynthesis, and even these only loosely identify precipitation, temperature, humidity and vegetation fluctuations as drivers of interannual variability in photosynthesis while their absolute effects and relative importance remain unclear [*Churkina and Running*, 1998; *Nemani et al.*, 2003; *Schaefer et al.*, 2002]. Also, being global in scope, such works tend toward broad-brush characterization of subcontinental-scale patterns [e.g., *Churkina and Running*, 1998; *Nemani et al.*, 2003; *Schaefer et al.*, 2002]. Thus much remains to be learned about how continental to regional productivity has responded to climate in recent decades, particularly for Africa.

[6] Comprehensive attribution of photosynthetic limitation by specific physiological and biophysical conditions is important in that it provides more detailed insight into likely effects of projected climate futures. For example, the 21st century is expected to bring decreased mean annual precipitation, increased air temperatures and a more variable hydrologic cycle with more extreme, persistent droughts for nearly the whole of Africa [*Intergovernmental Panel on Climate Change* (*IPCC*), 2001]. Land surface and ecosystem process models are instrumental in assessing which ecoclimatic or geographic regions are most vulnerable to projected climate changes, as well as the probable magnitude of associated water and carbon cycle excursions in response to climate change. However, insights gained from model applications are hindered by incomplete understanding of how modeled processes respond to unique sets of local environmental conditions.

[7] In this paper, we use a biophysical model, Simple Biosphere, Version 3 (SiB3), to study what drives spatiotemporal patterns of photosynthesis for ecoclimatic settings across the African continent during the period 1982–2003. We investigate physiological and biophysical drivers responsible for photosynthesis patterns in space and time, and provide an in-depth analysis of continental-scale carbon cycle dynamics with a particular focus on interannual variability. The approach enables attribution of variability in photosynthesis to specific weather and vegetation conditions and also reveals apparent inconsistencies between physiological and biophysical states that point to potential deficiencies in the model or its associated inputs. We address the following questions: (1) How large is interannual variation of photosynthesis across the African continent? (2) How much of this interannual variation is caused by physiological limitation (acute stress from low soil water, temperature, or low humidity) versus biophysical limitation (low vegetation radiation use)? (3) Which regions show the greatest interannual variability and why?

## 2. Methods

### 2.1. Model and Implementation

[8] The model Simple Biosphere, Version 3 (SiB3) is a land surface model originally designed [*Sellers et al.*, 1986] for use with General Circulation Models but used here in an "offline" mode to represent ecosystem physiology as driven by weather and vegetation. SiB [*Sellers et al.*, 1996a, 1996b, 1996c] estimates gross photosynthesis ($P$) with a modified version of *Farquhar et al.*'s [1980] model [*Collatz et al.*, 1991] scaled by the canopy integration scheme of *Sellers et al.* [1996c] and coupled to the Ball-Berry stomatal conductance model [*Ball et al.*, 1988; *Collatz et al.*, 1991, 1992]. Net photosynthesis ($P_{net}$) accounts also for the canopy-integrated leaf respiration, which is on the order of 10% of gross photosynthesis. Gross photosynthesis, net photosynthesis, and leaf respiration are scaled by stresses from the lack of soil water, high or low temperatures, and low air humidity as described further in Appendices A and B. SiB scales these "top leaf" photosynthetic rates to the canopy with the integration scheme of *Sellers et al.* [1992] that defines a canopy-scale, photosynthetically active radiation use parameter ($\Pi$) estimated from the fractional absorption of photosynthetically active radiation ($f_{PAR}$) derived from remotely sensed vegetation reflectances, here Normalized Difference Vegetation Index (NDVI), and vegetation type.

[9] The model's respiration rate depends on temperature and moisture and was scaled to produce annual balance with photosynthesis as by *Denning et al.* [1996]. This scaling is related to the model's lack of carbon pools then substituted by a first-order approximation that assumes respiration is driven by recent photosynthesis. Implemented as a calendar year annual balance the approach does not account for long-term sources and sinks. A recent addition to SiB partitions ecosystem respiration into autotrophic ($R_a$) and heterotrophic ($R_h$) components following *Schaefer et al.* [2008]. Among other things, this enables estimation of net primary production (NPP) from gross, canopy-scale photosynthesis minus autotrophic respiration ($NPP = P\Pi - R_a$). However, owing to uncertainty in the parameters controlling respiration's partition as well as weakness in the assumption of a calendar year balance between gross photosynthesis and ecosystem respiration, our analysis centers on photosynthesis terms and only examines NPP to place these results in the general context of those published. Still, favorable comparison between SiB's net ecosystem $CO_2$ exchange and that measured with the eddy covariance technique lends confidence to the model's process-level representation of ecosystem metabolism [*Colello et al.*, 1998; *Verma et al.*, 1992; *Baker et al.*, 2003; *Denning et al.*, 2003].

[10] The model's surface energy balance includes separate vegetation and ground temperatures that change according to net radiative input minus sensible and latent heat fluxes. The model's surface water balance is composed of canopy interception, ground ponding, soil, and snow balance equations that include inputs from precipitation or direct condensation, losses to evaporation, transpiration or

sublimation, as well as interlayer exchanges, where appropriate. Runoff occurs as deep gravity drainage and lateral flows during periods of infiltration excess.

[11] The newest version (SiB3) includes a prognostic canopy air space for temperature, moisture, and $CO_2$ [*Vidale and Stöckli*, 2005], and a 10-layer soil with explicit treatment of temperature and moisture based on the common land model [*Dai et al.*, 2003]. Also added is a mixed plant canopy physiology used here to simulate canopy-atmosphere exchanges for $C_3$ and $C_4$ plants separately [*Hanan et al.*, 2005], though they have the same soil water, radiation, and canopy air space environment.

[12] SiB3 was run for the period 1982–2003 with a 10-min time step on a 1° by 1° latitude/longitude grid encompassing the African continent. Model inputs for this implementation included soil texture [*Tempel et al.*, 1996], vegetation type [*DeFries et al.*, 1998; *Hansen et al.*, 2000], and the fraction of $C_4$ vegetation [*Still et al.*, 2003]. To obtain an observationally consistent vegetation parameterization, as well as phenomenologically correct soil water limitation of photosynthesis in the Sahelian zone (open savannas to the south of the Sahara desert) it was necessary to extend the coverage of short, wooded $C_4$ grassland further north to replace the $C_3$ bare soil parameterization that was prescribed in the original vegetation data set. This change is consistent with field observations of vegetation cover in the region. Surface weather was prescribed on the basis of the National Centers for Environmental Prediction Reanalysis 2 (data made available online by National Oceanic and Atmospheric Administration Climate Diagnostics Center, Boulder, Colorado, 2003). However, the 6-hourly precipitation was adjusted to obtain total monthly rainfall that matches the remote sensing plus gauge data merged Tropical Rainfall Measuring Mission (Tropical Rainfall Measuring Mission Science Data and Information System (TSDIS) Interface Control Specification, 2006, available at ftp://disc2.nascom.nasa.gov/data/TRMM/Gridded/3B43_V6/) 3B43 rainfall product for 1998 through 2003, or Climate Research Unit (CRU) [*Mitchell and Jones*, 2005; *New et al.*, 2000] monthly totals for 1982–1997 but adjusted to be consistent with the TRMM 3B43 monthly average spatial pattern from their period of overlap.

[13] The Simple Biosphere model contains algorithms, described by *Sellers et al.* [1994], *Los* [1998], and *Los et al.* [2000] for estimating a suite of light interception, surface roughness, resistance, and physiological parameters based on remotely sensed vegetation index. In this work we used the twice monthly, ~8 km NDVI made available by the Global Inventory Modeling and Mapping Studies (GIMMS) team [*Pinzon*, 2002; *Pinzon et al.*, 2005; *Tucker et al.*, 2006] derived from Advanced Very High Resolution Radiometer (AVHRR). While this NDVI data set contains corrections for satellite orbital drift, differing instrument calibrations, sensor degradation, and volcanic aerosols, we found large negative spikes of NDVI in many areas prone to cloud cover, and therefore replaced the lower 20% of NDVI of each biweek across years and at each ~8-km grid cell with the mean of the upper eighty percent. Furthermore, we found unusual seasonal dynamics in NDVI even after this lower fifth replacement, and discovered that this seasonal pattern is strongly anticorrelated with pyrogenic or dust aerosol contamination as seen from MODerate Resolution Imaging Spectroradiometer (MODIS) Terra Level-3 global, monthly atmospheric aerosol optical thickness (MOD08_M3). Therefore we performed an ad hoc adjustment to the AVHRR NDVI data so that their biweekly average seasonality matches the average seasonality seen with a filled, 5 km MODIS NDVI product (A. Huete, personal communication, 2006) covering the 5-year period of 2000–2004. This approach retains seasonal and interannual variability in NDVI and hence vegetation structure and function, but removes much of the erroneous seasonality associated with aerosol and water vapor contamination.

[14] Since each of these data sets (weather, soil type, vegetation type, NDVI, etc.) contains a unique resolution or grid, we selected a land point mask based on the 0.0727 degree by 0.0727 degree NDVI data set and regridded the other data sets to match this land point mask using a bilinear interpolation as needed, with the exception of vegetation type which was regridded on the basis of assignment of a nearest neighbor without interpolation. These 0.0727 degree data sets were then upscaled to the 1° grid again with bilinear interpolation except for vegetation type which was assigned the most frequent occurrence.

### 2.2. Analysis

[15] The core analysis in this paper quantifies limitation of canopy-scale photosynthesis by specific physiological and biophysical factors according to a procedure described briefly in words here and more formally in Appendix C. To put it simply, SiB calculates photosynthesis from the product of a physiologically defined rate with a biophysical effective area scaling that extends a single leaf's flux to the entire canopy. The model's diagnostics make it possible to calculate precisely how each biophysical and physiological factor limited photosynthesis in every time step and can be annually summed as performed here for a climatological analysis of what limits annual photosynthesis and drives its variability.

[16] On the physiological side, the leaf-scale gross photosynthetic rate ($P$) is reduced from a potential maximum ($P_{pot}$) according to multiplicative stress modifiers for temperature and soil water [*Sellers et al.*, 1996c] as well as regulation of intercellular $CO_2$ by stomatal closure [*Collatz et al.*, 1991, 1992; *Sellers et al.*, 1992, 1996c]. On the biophysical side, the canopy-scaling parameter ($\Pi$) is reduced from its potential maximum ($\Pi_{max}$). Appendix A describes biophysical and physiological terms, and Appendix B defines and illustrates stress controls. Combining the physiological and biophysical conditions, canopy-scale gross photosynthesis is obtained from $P\Pi$ (analogous to what many would define as gross primary productivity) and it has a potential maximum value of $P_{pot}\Pi_{max}$.

[17] It is important to notice the model's joint limitation of canopy-scale photosynthesis by physiology and biophysics according to the product $P\Pi$. A key consequence of this feature for the current analysis is that the magnitude of limitation by physiology depends on the biophysical state and vice versa. In other words, the marginal photosynthesis return from additional water depends on leaf area extent, and similarly the marginal photosynthesis return from additional leaves depends on the plant physiological state such as hydration. This highlights a point of departure

**Table 1.** Statistics for Africa-Wide, Biome-Specific Net Primary Productivity Estimated With SiB, Presented as Means, Standard Deviations, and Coefficient of Variation Both per Unit Area and Total[a]

| Biome | Mean NPP (kg C $m^{-2}$ $a^{-1}$) | SD NPP (kg C $m^{-2}$ $a^{-1}$) | CV NPP | $NPP_{tot}$ (Pg C $a^{-1}$) | SD $NPP_{tot}$ (Pg C $a^{-1}$) | CV $NPP_{tot}$ | Fraction of Africa's $NPP_{tot}$ | Fraction of Africa's NPP |
|---|---|---|---|---|---|---|---|---|
| Evergreen Broadleaf | 1.65 | 0.11 | 0.07 | 4.14 | 0.12 | 0.03 | 0.25 | 0.08 |
| Deciduous Broadleaf | 1.31 | 0.13 | 0.10 | 0.45 | 0.02 | 0.04 | 0.03 | 0.01 |
| Cropland | 1.13 | 0.12 | 0.10 | 1.04 | 0.04 | 0.04 | 0.06 | 0.03 |
| Woodland | 0.88 | 0.11 | 0.12 | 5.12 | 0.21 | 0.04 | 0.31 | 0.19 |
| Savanna | 0.65 | 0.09 | 0.14 | 4.86 | 0.28 | 0.06 | 0.29 | 0.25 |
| Shrubland[b] | 0.07 | 0.02 | 0.29 | 1.00 | 0.12 | 0.12 | 0.06 | 0.45 |
| All Biomes | 0.53 | 0.07 | 0.12 | 16.60 | 0.57 | 0.03 | 1.00 | 1.00 |

[a]Here CV is the coefficient of variation. Here NPP represents the net primary productivity per unit area and $NPP_{tot}$ represents the net primary productivity per unit total. The contribution of each biome to average NPP in Africa is also shown with percent of land area for comparison.
[b]Includes effectively bare soil regions such as much of the Sahara.

between models that grow vegetation from photosynthesis and are inherently consistent with climate compared to models like SiB that prescribe vegetation dynamics from observations. The latter class of models risks inconsistency between prescribed vegetation and climate driven parameterizations of stress (Either the prescribed vegetation is wrong or the parameterization of the effects of climate is wrong, e.g., plant water stress parameterization is wrong and/or precipitation is wrong). In contrast, dynamic vegetation models force vegetation to match their particular parameterization of climate driven stresses even if either or both are wrong.

[18] One advantage to prescribing vegetation from observations is its ability to capture the real suppression of canopy-scale photosynthesis where vegetation is sparse in spite of conditions that may favor more extensive vegetation cover. This could arise where human or natural disturbances lower vegetation density, a process that is not captured in ecosystem process models that grow vegetation that is inherently consistent with a recent history of weather/climate. While prescribing vegetation can complicate attribution it also presents an opportunity for exposing apparent inconsistencies. For example, a case of very high stress coincident with a highly vegetated state would seem unsustainable from a biological point of view as chronic stress would cause vegetation dieback. Alternatively, the case of anomalously low stress with low vegetation is also inconsistent as vegetation is expected to more completely use available resources for photosynthetic gain. Such apparent inconsistencies are revealed by our analysis and help us to learn about potential model or model input errors, or missing processes (e.g., land use).

## 3. Results

### 3.1. Spatial Pattern of Photosynthesis Across Africa

[19] Annual net primary productivity (NPP) averages 16.6 Pg C $a^{-1}$ (where a is years) for the African continent (Table 1), greater than other published model estimates that range 7 to 13 Pg C $a^{-1}$ [*Cramer et al.*, 1999; *Potter*, 1999; *Cao et al.*, 2001; *McGuire et al.*, 2001; *Potter et al.*, 2003]. The relatively high estimates in this study are likely due to the following three factors unique to this model application: (1) monthly rainfall totals were nudged to match the TRMM and CRU patterns which tended to increase rainfall across the continent; (2) remotely sensed NDVI was, on average, increased to partially correct for aerosol contamination; and (3) $C_4$ photosynthesis is explicitly included. Evergreen broadleaf forest, closed woodland, and savanna biomes each account for roughly 30% of this total continental NPP, with increasing surface area offset by decreasing photosynthesis leading to nearly equal biome total contributions. Combined, these biomes account for nearly all (~85%) of the continent's photosynthesis (Table 1). General continental patterns agree with those reported in previous global applications of process models [*Cramer et al.*, 1999; *Potter*, 1999; *Cao et al.*, 2001; *McGuire et al.*, 2001; *Potter et al.*, 2003]. The standard deviation of annual NPP increases roughly linearly with its mean (Table 1) but saturates at high photosynthesis (evergreen broadleaf forests). Not surprisingly, the coefficient of variation in NPP decreases roughly linearly with biome-averaged annual NPP except for shrublands and bare soil where variability is a relatively large fraction of small averages.

[20] Interannual variability in net primary productivity was estimated to be 0.6 Pg C $a^{-1}$ continent wide, which is rather small considering reports of the same or larger magnitude variability in continent-wide net ecosystem $CO_2$ exchange [*McGuire et al.*, 2001; *Williams et al.*, 2007]. However, unlike in other model implementations, respiration is rescaled in this application to obtain an annually carbon-balanced biosphere, which acts to dampen this study's estimate of the interannual variability in NPP.

[21] Focusing on net photosynthesis alone ($P_{net}$ defined above), areas with high interannual variability of $P_{net}$ are concentrated south of the equator (Figure 1a). A notably similar spatial pattern of IAV is found for evapotranspiration (Figure 1c), owing to physiological coupling of water and carbon fluxes. In contrast with this regional-scale hot spot of absolute year-to-year variation in net photosynthesis, the coefficient of variation highlights dryland and desert margins of the Sahara, Sahel, Namib, Kalahari, and the Greater Horn of East Africa (Figure 1b). Though the coefficient of variation in photosynthesis is certainly of importance with regard to food production and supply, the absolute variability is more relevant to the challenge of understanding variability in global sources and sinks of carbon dioxide, the primary focus of this work.

[22] Comparing the spatial pattern of IAV in precipitation (Figure 1d) with that for photosynthesis (Figure 1a), rainfall variability alone is clearly not enough to explain the regional hot spots of variability. For example, in parts of West Africa where the IAV of precipitation is high, photo-

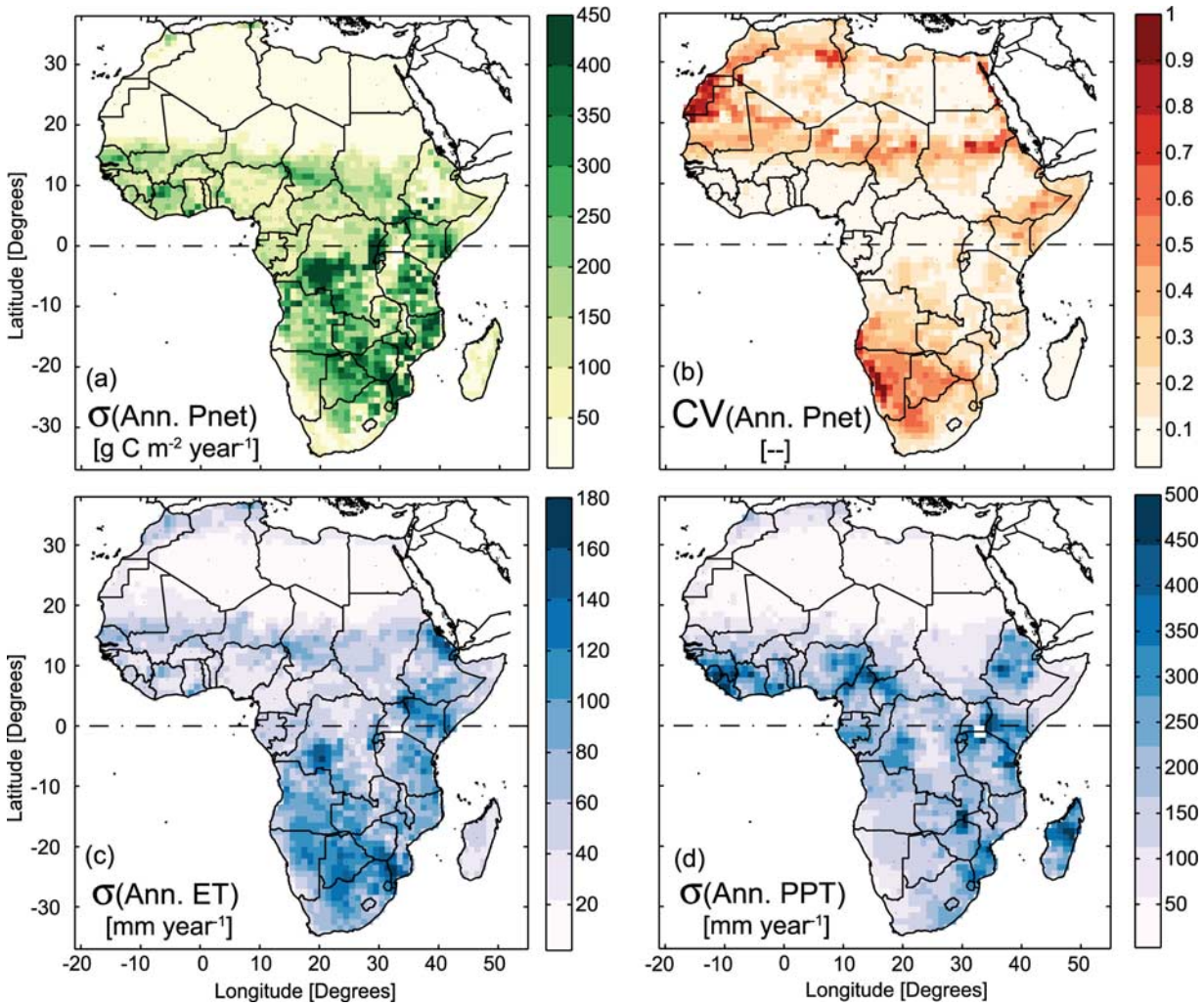


**Figure 1.** Spatial distribution across Africa of (a) standard deviation ($\sigma$) of annual net photosynthesis ($P_{net}$), (b) coefficient of variation of annual net photosynthesis, (c) standard deviation of annual evapotranspiration, and (d) standard deviation of annual precipitation (PPT).

synthesis has only modest variability (further discussion in section 3.3). To better diagnose what drives interannual variation in photosynthesis we study to what degree acute stresses or $f_{PAR}$ limit photosynthesis and how much they induce year-to-year variation.

### 3.2. Drivers of Variability in Photosynthesis Across Africa

[23] Figure 2 presents the reduction of canopy-scale gross photosynthesis from its biochemically limited and light-limited potential rate expressed in absolute (Figures 2–2d) as well as relative to the total reduction (Figures 2e–2h). This quantifies the degree to which soil water scarcity, low air humidity, high (or low) temperatures, or the lack of $f_{PAR}$ limit modeled photosynthesis. Immediately evident is the shared importance of $f_{PAR}$ and soil water limitation across much of the dryland regions of the continent (Figures 2a, 2b, 2e, and 2f). However, sizable limitation by acute soil water stress extends far into the equatorial zone of southern Africa, while $f_{PAR}$ limitation is relatively large throughout most of West Africa as well as parts of East Africa. Limitation by heat stress is modest to absent except in a belt across the Sahara desert as well as a portion of southern and eastern African drylands (Figures 2c and 2g). Humidity stress is essentially absent across the continent, with its greatest influence in the forest zone of equatorial Central Africa where the absolute reduction is very modest (Figures 2d and 2h). The blocky pattern appearing in absolute reductions (Figures 2a and 2b) derives from more extensive prescription of $C_4$ vegetation across the Sahelian zone, but this has only subtle influence on the relative reduction of canopy-scale gross photosynthesis.

[24] Figure 3 presents the interannual variability in limitation of gross photosynthesis by each factor expressed in absolute (Figures 3a–3d) as well as relative to the total interannual variability (Figures 3e–3h). Soil water scarcity drives almost all of the interannual variability of gross photosynthesis (Figure 3b), with $f_{PAR}$ limitation (Figure 3a) accounting only for the modest IAV of photosynthesis in the moist tropical forest regions close to the equator and on the Guinea coast of West Africa.

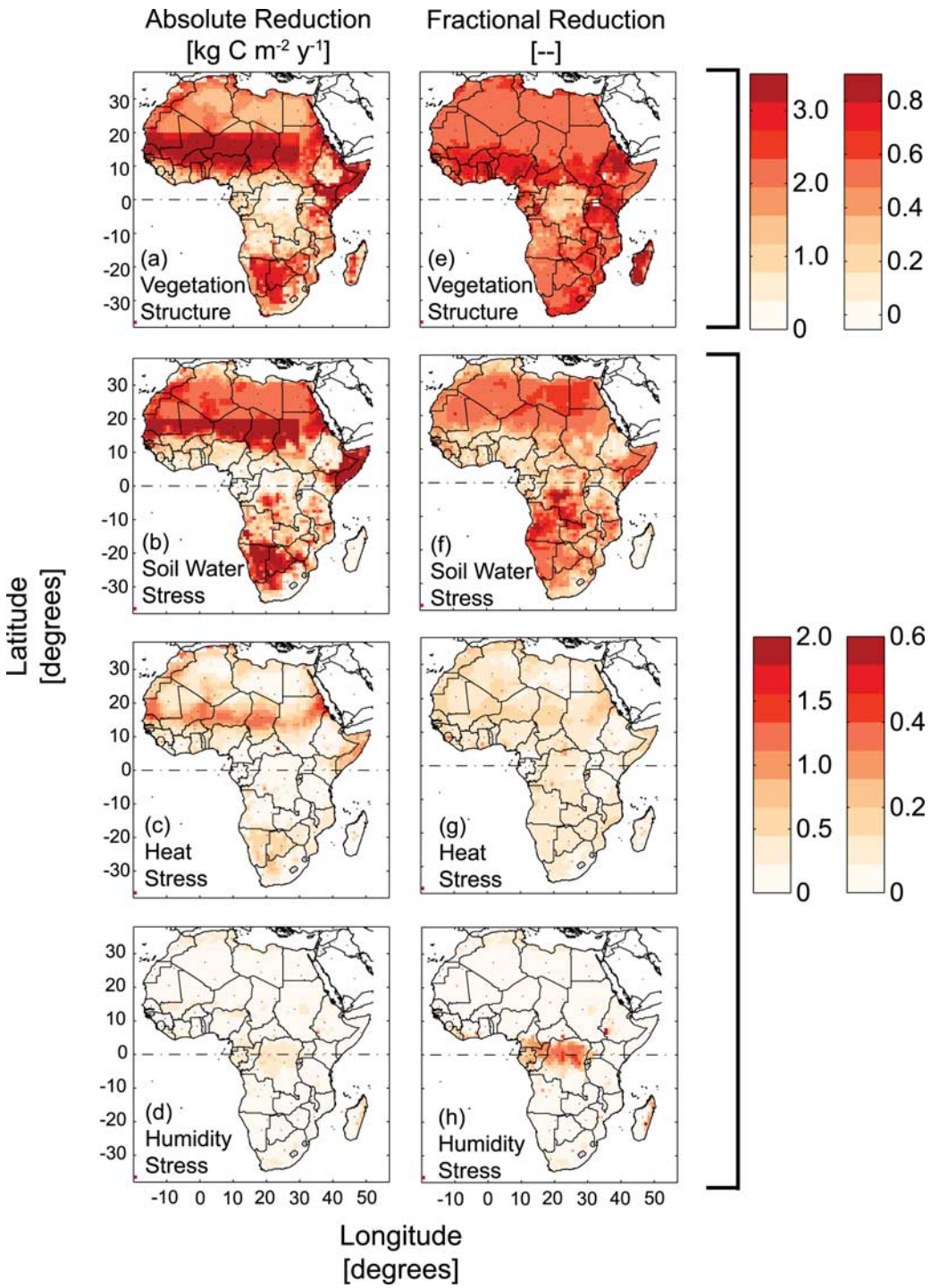


**Figure 2.** Spatial distribution across Africa of the reduction of mean annual gross canopy photosynthesis from its potential rate expressed in (a–d) absolute (left color bars) and (e–h) fraction of total (right color bars) terms associated with vegetation structure (Figures 2a and 2e), soil water stress (Figures 2b and 2f), heat stress (Figures 2c and 2g), or humidity stress (Figures 2d and 2h).

Interestingly, interannual variability in soil water stress (Figure 3b) tends not to be highest in places that have the largest interannual variability in precipitation (Figure 1d) but rather at intermediate values, as water ceases to be a limiting factor with increasing rainfall despite continued increase in rainfall variability. Acute heat and humidity stresses induce almost no interannual variability in photosynthesis (Figures 3c and 3d).

[25] Figure 4 simplifies these details by expressing the factor that is most limiting (Figure 4a) or that induces the greatest interannual variability (Figure 4b). The prevailing condition of limitation by $f_{PAR}$ indicates that vegetation

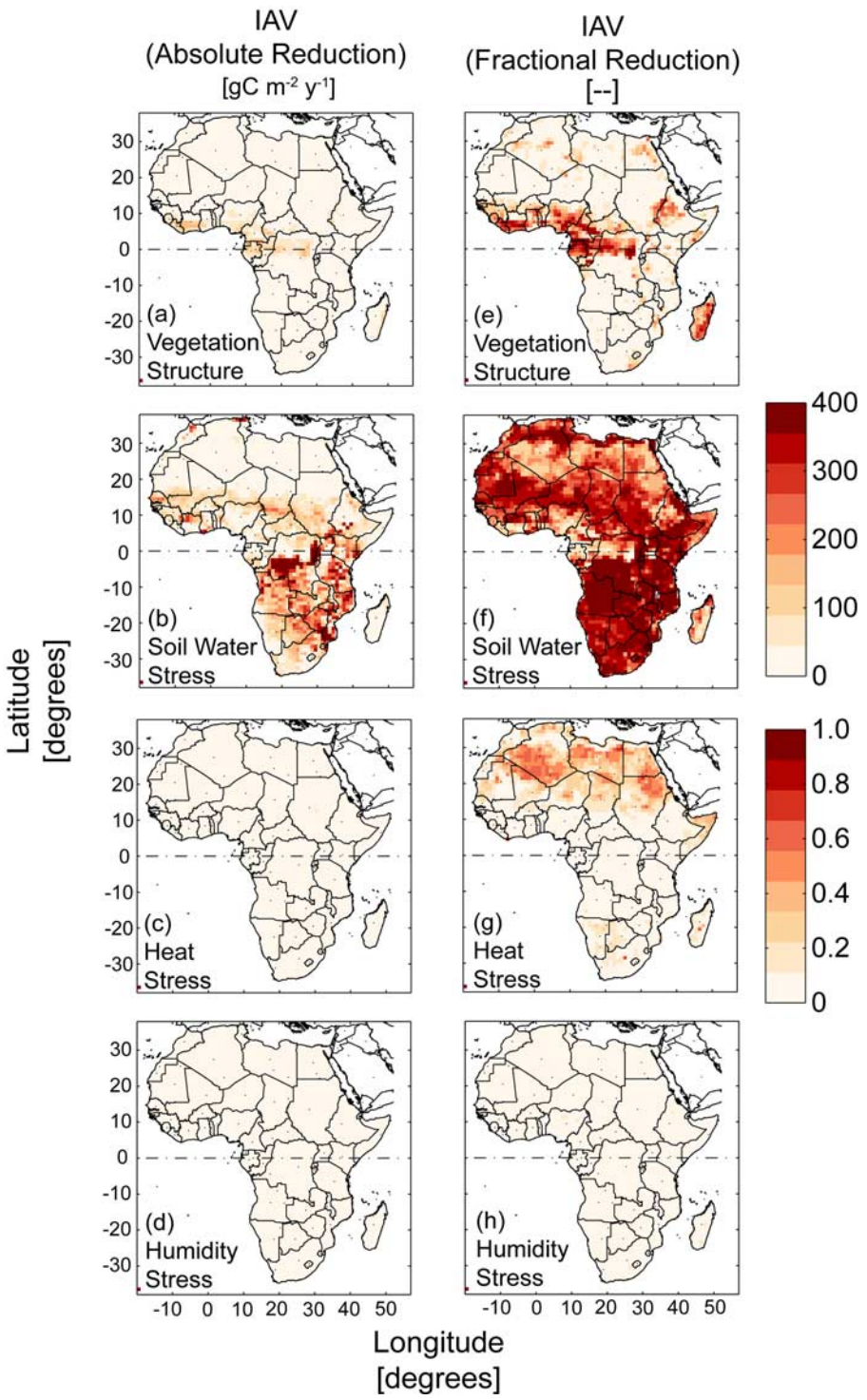


**Figure 3.** Spatial distribution across Africa of the interannual variability in the reduction of gross canopy photosynthesis from its potential rate expressed in (a–d) absolute (top color bar) and (e–h) fraction of total (bottom color bar) terms associated with vegetation structure (Figures 3a and 3e), soil water stress (Figures 3b and 3f), heat stress (Figures 3c and 3g), or humidity stress (Figures 3d and 3h).

density is generally consistent with avoidance of chronic stress under average climate conditions. Notably large constraint by $f_{PAR}$ in parts of West and East Africa compared to regions of similar vegetation and rainfall conditions in the south could indicate that climate conditions can support more vegetation than is observed in the former and point to an apparent inconsistency as described in section 2.2. In contrast, parts of southern Africa where soil water is the primary limiting factor may have a vegetation density that exceeds what is typically supported by the

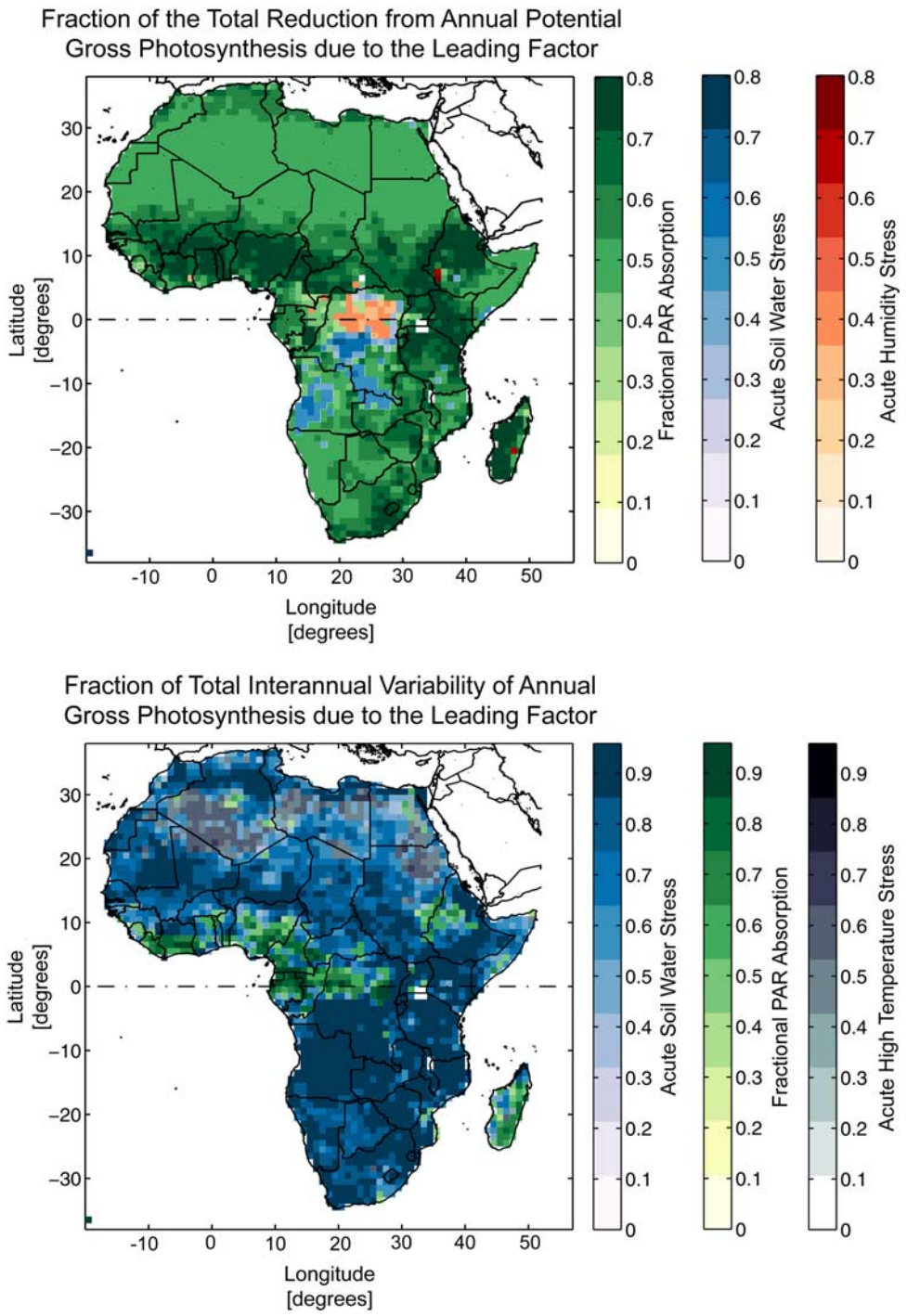


**Figure 4.** Spatial distribution across Africa of (top) the fraction of the total reduction from potential annual gross canopy photosynthesis associated only with the "leading" factor that exerts the greatest limitation and (bottom) the fraction of total interannual variability of gross canopy photosynthesis associated only with the leading factor that induces the greatest interannual variability.

region's climate with the possibility for vegetation decline. These particular features may indicate model or model input errors if not the absence of real processes such as land use disturbances that reduce vegetation from what could be supported by the prevailing climate.

[26] Nearly all of the continent's interannual variability in photosynthesis is governed by variation in soil water availability (Figure 4b), with variation in $f_{PAR}$ becoming important only in very wet locations (>1.5 m of rainfall per year). This result together with prevailing limitation by $f_{PAR}$ (Figure 4a), suggests that while vegetation density reflects the biological necessity of avoiding a persistent state of physiological stress, it is also extensive enough to be highly

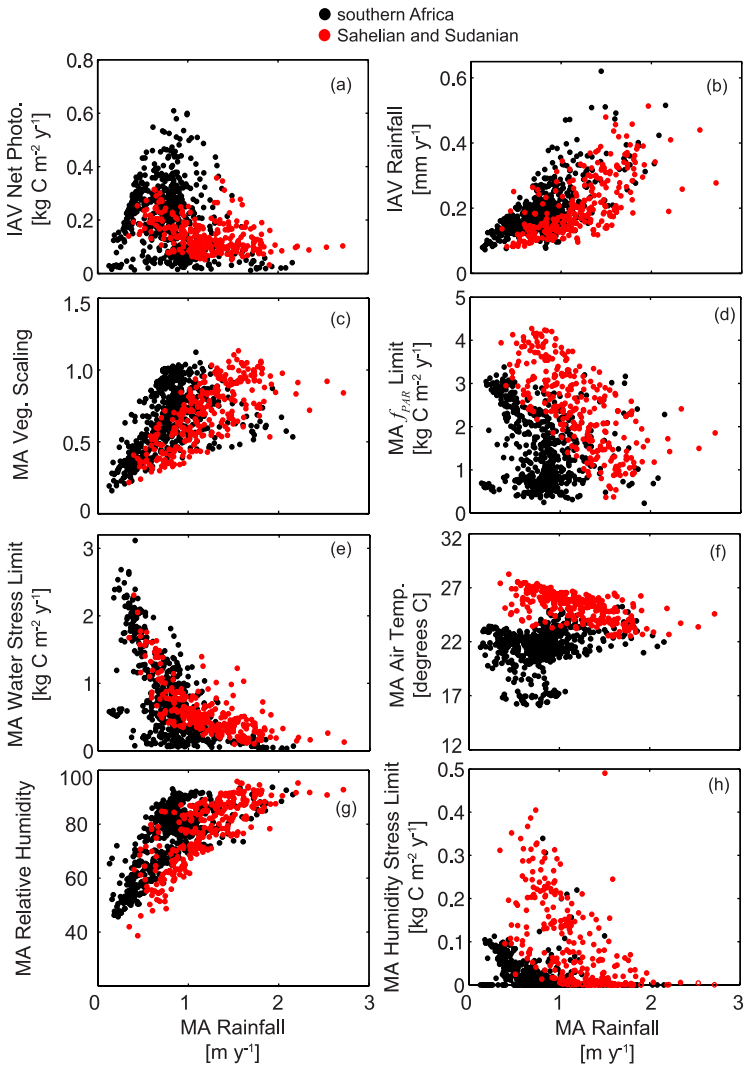


**Figure 5.** State space plots of ecoclimatic conditions versus mean annual rainfall for woodland and savanna grid cells of Africa south of the equator or southern Africa (black) and the Sahelian to Sudanian zone (red). IAV is the interannual variability, expressed as the standard deviation of annual values; MA is the mean annual; Net Photo, is the net photosynthesis; and Air Temp is the air temperature. Relative humidity and air temperature are weighted by each month's fraction of total annual potential canopy-scale photosynthesis to emphasize the growing season conditions.

sensitive to water limitation, responding to relatively wet episodes and suffering from dry spells.

### 3.3. Contrasting Southern and Northern Woodlands and Savannas

[27] Deeper exploration is required to explain why year-to-year variation in $P_{net}$ is lower in the northern Sudano-Sahelian zone compared to southern woodlands and savanna (Figures 1a and 5a), despite comparable if not higher mean annual $P_{net}$ as well as still large variability in annual rainfall for northern drylands (Figure 5b). Three features explain this outcome, lower $f_{PAR}$, lower rainfall variability, and a hotter, dryer climate in the Sudano-Sahelian zone. The most important of these features is lower PAR absorption resulting in higher mean annual $f_{PAR}$ limitation for the same mean annual rainfall in the Sudano-Sahelian zone compared to southern woodlands and savannas (Figures 5c and 5d). This could simply be exposing errors in prescribed weather or vegetation (NDVI). However, it is more likely the expression of a real land use or ecoclimatic phenomenon. Low $f_{PAR}$ could derive from more intense land use pressure from grazing, wood harvest, or agriculture, broadly consistent with *Imhoff et al.* [2004] who report relatively high human consumption of plant productivity in the Sudano-Sahelian zone compared to parts of southern Africa. In addition, several recent studies have documented broad increases in satellite vegetation indices in the Sahel and Sudanian zones [*Nicholson et al.*, 1998; *Prince et al.*, 1998; *Herrmann et al.*, 2005; *Olsson et al.*, 2005; *Prince et al.*, 2007] and increasing woody cover following the droughts of the 1970s and 1980s. Thus our inferred $f_{PAR}$ limitation may reflect historic drought suppression of vegetation that is starting to recover in later years.

[28] Alternatively, climatic differences may be partially or wholly responsible for regional differences in photosynthetic

limitations. While mean annual limitation by acute soil water stress is similar (Figure 5e), the Sudano-Sahelian drylands experience higher temperatures (Figure 5f) and lower relative humidity (Figure 5g) together causing greater evaporative demand and higher humidity stress (Figure 5h). Mechanistically, reduction of photosynthesis from its potential rate by either humidity stress or low $f_{PAR}$ have the direct effect of reducing the range over which $P_{net}$ can vary with soil water status thus dampening $P_{net}$ responses to soil water stress. Furthermore, both low $f_{PAR}$ and humidity stress suppress transpiration during wet conditions, which combines with the high resistance of dry surface soils to restrict evapotranspiration driven reductions in soil water. This secondary effect allows soil water to stay unusually high, artificially alleviating soil water stress during successive ''green'' or more humid periods and thus further diminishing $P_{net}$ sensitivity to variability in rainfall. In addition to these biophysical explanations, Sudano-Sahelian drylands also have a slightly lower interannual variability in rainfall for the same mean annual rainfall compared to drylands of southern Africa (Figure 5b) according to the spatial patterns in the CRU and TRMM rainfall data sets used in this study. Soil physical / hydraulic parameterization and associated soil water stress sensitivity of photosynthesis do not differ between the regions.

## 4. Discussion

[29] Acute water stress emerges as the primary factor governing the magnitude of IAV in photosynthesis across Africa. Interannual variability in rainfall does not necessarily induce IAV of plant water stress, as net photosynthesis in some of the wettest places is largely insensitive to IAV of rainfall (Figure 6). Thus to understand carbon cycle sensitivity to drought cycles and precipitation variability, it is important to consider how vegetation, soil, and other climatic conditions may filter or dampen this variability through a finite storage volume coupled with the nonlinearity of photosynthesis response to soil water. The highest year-to-year variability of annual $P_{net}$ occurs in places with intermediate annual rainfall, intermediate variability of annual rainfall, and also high potential canopy-scale photosynthesis (annual $P_{pot}$) (Figure 6), where $P_{pot}$ depends on light intensity and duration, vegetation-specific and temperature-dependent reaction rates, and vegetation density. Observations at long-term ecological research sites across North America report the same pattern [*Knapp and Smith*, 2001] of a peak in the interannual variability of aboveground net primary production where precipitation variability is intermediate, not maximum, as well as where potential growth rate is high. Identifying such hot spots requires consideration not only of rainfall variability, but also the full ecohydrological setting that receives these fluctuations.

[30] Focus in this work on photosynthesis rather than other components of ecosystem metabolism (respiration, fire) or their net balance stems from a lack of confidence in the ability of biophysical models to capture interannual dynamics of these other carbon cycle processes. Since respiration anomalies tend to be positively correlated with anomalies of photosynthesis [e.g., *Barr et al.*, 2007; *Reichstein et al.*, 2007] variability in photosynthesis is likely to be severely damped as it is expressed in net ecosystem exchange. However, a lag in fire or respiration responses to climate fluctuations, say through net ecosystem carbon storage in wet periods and release in dry periods, could permit the propagation of gross anomalies through to net ecosystem exchange. In fact, if the gross uptake and release processes were completely out of phase but close to a long-term balance, anomalies of net ecosystem exchange would be twice those of photosynthesis. Though not mechanistically plausible it raises the point that photosynthesis alone is insufficient for quantifying interannual variability in *NEE* and that it is crucial we better understand interannual variability of respiration and fire. Still, detailed understanding of how photosynthesis responds to climate fluctuations is needed to anticipate likely carbon cycle responses to global change and to identify regions that may be particularly vulnerable.

[31] Model results presented here generate some interesting hypotheses that can only be tested with new observations. In particular, results highlighted lower vegetation density for a given rainfall regime in West Africa compared to southern Africa. The model also suggests slightly higher though still modest humidity stress in the Sudanian-Sahelian zones in comparison to that in southern Africa. Do low vegetation density and humidity stress in fact dampen the ecophysiological sensitivity to rainfall variability? Widespread observations are needed to determine if the meteorology or vegetation prescribed for the region is severely flawed. Process representation in the model may also be inadequate (or incorrect), calling for further model testing with land surface flux and state observations such as provided with the eddy covariance technique. Prescription of absorbed PAR could be evaluated with new or existing vegetation surveys or with remotely sensed vegetation cover products that are independent of the AVHRR NDVI data set used here. Leaf- and canopy-scale observations of ecophysiology throughout the region should provide the data needed to test regional application of the model's global, biome-scale parameterization of physiological stresses. Fortunately, recent instrumental deployments and field campaigns currently underway hold promise for addressing this need. Still, it is possible that the model's process-level representation and prescribed weather and vegetation correctly capture a lack of absolute, though still large relative, interannual variability in photosynthesis throughout the Sahelian to Sudanian zones compared to that in southern Africa's woodlands, savannas, and grasslands.

[32] With a brief look to the future, climate models project an amplification of drought cycles and higher temperatures for much of the continent [*IPCC*, 2001]. Extrapolating from this historical analysis to hypothesize about possible responses to these trends, the IAV of photosynthesis may simply grow in proportion to its locally defined sensitivity with the largest response anticipated for regions of intermediate annual rainfall and high photosynthetic potential (Figure 6). In contrast, absolute variation in annual photosynthesis for the driest regions in and around deserts and the wettest regions such as the Guinean zone and Congo basin are expected to be largely insensitive to such perturbations by climate excursions. In fact, higher temperatures could increase humidity stress in

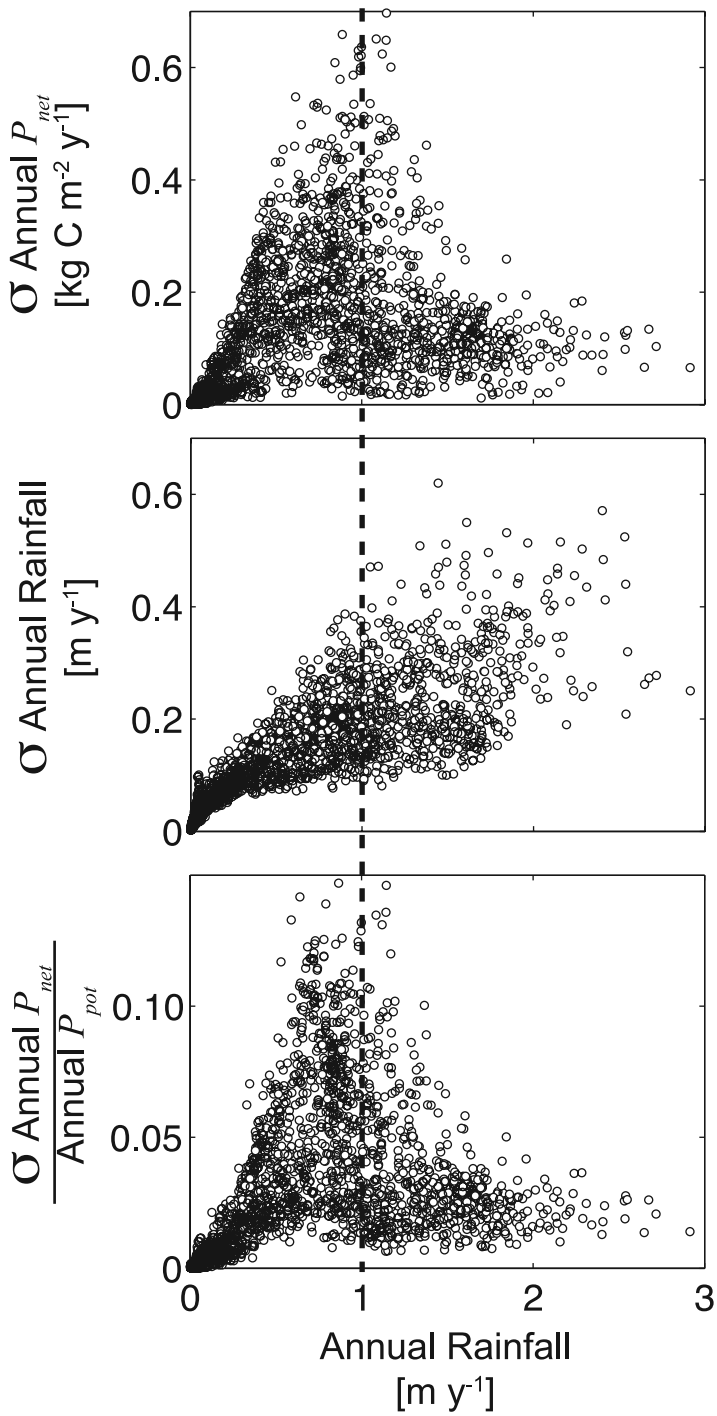


**Figure 6.** Distribution with annual rainfall of (top) the standard deviation of annual canopy-scale net photosynthesis, (middle) the standard deviation of annual rainfall, and (bottom) the ratio of the standard deviation of annual canopy-scale net photosynthesis to potential annual gross photosynthesis, each shown for all grid cells across Africa.

much of the Guinean and Sudanian zones, possibly reducing the region's IAV of photosynthesis. Still, the net continental-scale effect on photosynthesis of an increase in temperature is unclear as it likely depends on the balance between some places losing sensitivity as they enter a state of perpetual water scarcity as opposed to other places that gain sensitivity owing to more frequent, longer duration periods of water stress caused by increased evaporative demand and/or reduced water availability.

## 5. Conclusions

[33] Acute soil water stress emerges as the primary factor driving interannual variability of photosynthesis for most of the African continent. In contrast, modeled average annual

productivity is limited by vegetation PAR absorption as prescribed from remotely sensed vegetation index. Put together these results suggest that while vegetation density reflects the biological need to avoid a persistent state of physiological stress, it is also extensive enough to use resources intensively and thus is highly sensitive to departure from the long-term average climate. Photosynthesis exhibits the greatest interannual variability in southern savannas and woodlands where photosynthetic potential is high but rainfall variability and annual rainfall are both intermediate. Relatively low vegetation cover, pronounced humidity stress, and somewhat lower rainfall variability diminish interannual variability of photosynthesis in much of the Sudano-Sahelian zone, as do perennially wet conditions in much of the Congo Basin and coastal West Africa. These findings underscore the importance of considering how vegetation, climate, and soil characteristics may filter or dampen ecosystem responses to hydroclimatic variability. Furthermore, model results generate hypotheses that draw attention to the need for an expanded network of ecophysiological and biophysical observations across the continent.

## Appendix A

[34] SiB3 calculates the potential top leaf gross photosynthetic rate ($P_{\text{pot}}$) as the quadratically smoothed minimum of the light-, Rubisco-, and export-limited assimilation rates ($w_e$, $w_c$, $w_s$) from *Collatz et al.*'s [1991, 1992] version of *Farquhar et al.*'s [1980] photosynthesis model using an unstressed maximum catalytic capacity of Rubisco ($V_{\text{max}}$) without stomatal limitation. The model calculates the "realized," fully stressed gross photosynthesis ($P$) iteratively to include reduction in the catalytic capacity of Rubisco according to multiplicative stress modifiers for temperature ($M_T$) and soil water ($M_w$) [*Sellers et al.*, 1996c] as well as reduction due to regulation of intercellular $CO_2$ by stomatal closure [*Collatz et al.*, 1991, 1992; *Sellers et al.*, 1992, 1996c], each described more fully in Appendix B. SiB3s net photosynthesis ($P_{\text{net}}$) also accounts for leaf respiration [*Collatz et al.*, 1991, 1992; *Sellers et al.*, 1992, 1996c] that is on the order of 10% of $P$ and that is similarly dependent on multiplicative temperature and soil water stress modifiers.

[35] As an intermediate diagnostic, SiB3 also calculates the water plus temperature stressed gross photosynthetic rate at a leaf surface relative humidity of 100% ($P_{ci}$), omitting stomatal limitation according to

$$C_i = C_s - \frac{P_{\text{net}}}{\frac{m P_{\text{net}}}{C_s} + b}, \tag{A1}$$

where $C_i$ and $C_s$ are partial pressures of $CO_2$ in the leaf intercellular cavity and at the leaf surface, and the $m$ and $b$ are parameters determined empirically on the basis of leaf gas exchange measurements of $P_{\text{net}} - C_i$ behavior. This $P_{ci}$ intermediate between $P_{\text{pot}}$ and $P$ enables quantification of the degree to which photosynthesis is limited by humidity stress versus water plus temperature stress as described in Appendix C. Separating limitation by temperature versus water stress (also in Appendix C) requires the use of control coefficients ($O_x$) [e.g., *Woodrow and Berry*, 1988] that capture the degree to which the smoothed minimum of the three potential photosynthesis rates was influenced by the Rubisco- and PEP/sink-limited rates relevant for each type of stress

$$O = \frac{\partial P_{ci}}{\partial w}\frac{w}{P_{ci}}, \qquad O_e + O_c + O_s = 1. \tag{A2}$$

SiB3 scales the top leaf photosynthesis rates described above with a leaf-to-canopy scaling parameter, $\Pi = f_{\text{PAR}} / k$, where $k$ is a dynamic coefficient of PAR extinction within the canopy accounting for the latitudinally and diurnally varying insolation angle and biome-dependent canopy structural properties such as leaf angle. $\Pi_{\text{max}}$ is the value obtained when $f_{\text{PAR}}$ is its maximum of 0.95. Thus the maximum canopy-scale photosynthesis rate is $P_{\text{pot}}\Pi_{\text{max}}$ and the fully stressed, realized canopy-scale photosynthesis rate is $P\Pi$.

## Appendix B

[36] Figure B1 illustrates the how acute stresses limit photosynthesis as it responds to environmental conditions. Beginning with response to temperature, consistent with *Sellers et al.* [1996c], high and low temperature inhibitions reduce photosynthesis according to the multiplicative reduction functions

For $V_m$ of $C_3$ photosynthesis

$$M_T = \frac{2^{Q_t}}{(1 + \exp[s_1(T_c - s_2)])},$$

For sink-limited rate of $C_3$ photosynthesis

$$M_T = \frac{2^{Q_t}}{(1 + \exp[s_3(s_4 - T_c)])}, \tag{B1}$$

For $V_m$ of $C_4$ photosynthesis

$$M_T = \frac{2^{Q_t}}{(1 + \exp[s_1(T_c - s_2)])(1 + \exp[s_3(s_4 - T_c)])},$$

For $V_m$ of canopy respiration

$$M_T = \frac{2^{Q_t}}{(1 + \exp[s_5(T_c - s_6)])},$$

where $Q_t$ is $0.1(T_c - 298)$, $T_c$ is canopy temperature, and $s_i$ are high and low temperature inhibition parameters. The combination of low temperature and high temperature inhibitions produces a peaked curve (Figure B1a) with higher rates for $C_4$ than $C_3$ at high temperatures and the reverse at lower temperatures.

[37] Photosynthesis also depends on plant available water (Figure B1b) according to the multiplicative soil water stress factor

$$M_w = \frac{(1 + s)W}{s + W}, \tag{B2}$$

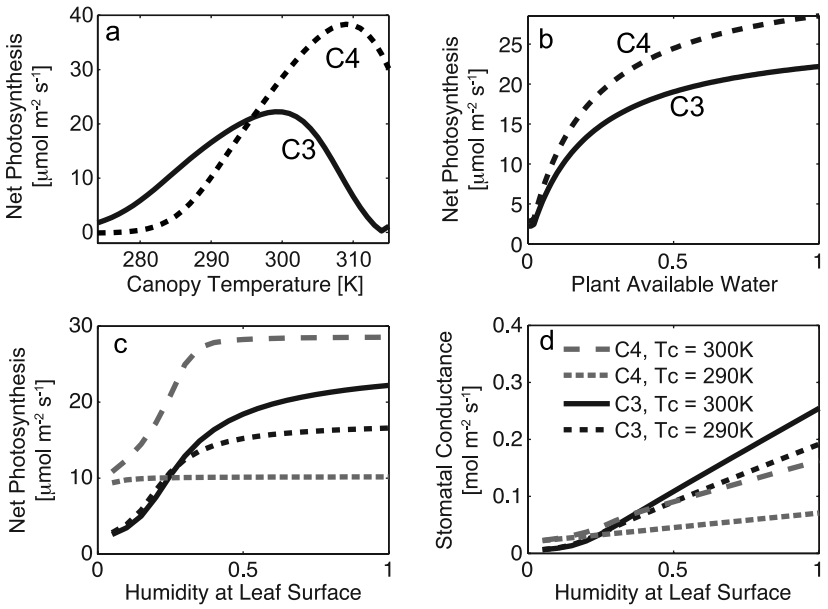


**Figure B1.** Response of light-saturated net photosynthesis to instantaneous environmental conditions of (a) canopy temperature ($T_c$) with $h_s = 1$ and no water stress, (b) plant available water with $h_s = 1$ and $T_c = 300$ K, (c) humidity with no water stress, and (d) the response of stomatal conductance to humidity. Mixed forest parameters (SiB2 biome 3) were used for $C_3$ and wooded grassland parameters (SiB2 biome 7) for $C_4$ and $\Pi = 1$.

where $s$ is a shape parameter set to 0.2, and $W$ is the ratio of plant available water in the root zone minus the plant available water at the field capacity soil water potential, with plant available water defined as the vertically integrated volume of water in the soil's root zone minus that at the wilting point soil water potential. The plant available water ratio is allowed to range 0 to 1.

[38] In the case of humidity stress, the model solves for a net photosynthesis-leaf intercellular partial pressure of $CO_2$ ($C_i$, Pa) pair that satisfies a slightly modified form of the "Ball-Berry" equation for $C_3$ or $C_4$ vegetation [*Ball et al.*, 1988; *Collatz et al.*, 1991, 1992]

$$g_s = m\frac{P_{\text{net}}h_s}{C_i}p + bLM_w, \tag{B3}$$

where $g_s$ is stomatal conductance that the model uses prognostically from the previous time step, $h_s$ is relative humidity at the leaf surface, $p$ is atmospheric pressure [Pa], $m$ and $b$ are parameters determined empirically on the basis of leaf gas exchange measurements of $P_{\text{net}} - C_i$ behavior and assigned 9 and 0.01 for $C_3$, or 4 and 0.04 for $C_4$, and $L$ is total photosynthetically active leaf area [$m^2$ leaf $m^{-2}$ ground]. Correspondingly, net photosynthesis and stomatal conductance of $C_3$ vegetation are more sensitive to humidity, however at high temperature and low humidity the absolute reduction of $C_4$ net photosynthesis can also be large (Figures B1c and B1d).

## Appendix C

[39] The total reduction of canopy-scale photosynthesis from its potential, canopy-scale rate ($P_{\text{pot}}\Pi_{\max} - P\Pi$, see Appendix A) is composed of the following two elements: (1) the physiological reduction of the top leaf photosynthetic rate from $P_{\text{pot}}$ to $P$ caused by acute temperature stress, water stress, or low humidity and (2) the biophysical reduction of canopy radiation use from $\Pi_{\max}$ to $\Pi$ related to canopy extent. Each component of the total reduction can be written as a fraction ($Y_{\text{acute}} = 1 - P/P_{\text{pot}}$ and $Y_{\text{veg}} = 1 - \Pi/\Pi_{\max}$), and their relative influences are quantified by proportionalities, as

$$F_{\text{acute}} = \frac{Y_{\text{acute}}}{Y_{\text{acute}} + Y_{\text{veg}}}, \quad F_{\text{veg}} = \frac{Y_{\text{veg}}}{Y_{\text{acute}} + Y_{\text{veg}}}. \tag{C1}$$

Absolute reductions attributed to acute stress or canopy radiation use are then calculated as

$$S_{\text{acute}} = F_{\text{acute}}\left(P_{\text{pot}}\Pi_{\max} - P\Pi\right), \quad S_{\text{veg}} = F_{\text{veg}}\left(P_{\text{pot}}\Pi_{\max} - P\Pi\right). \tag{C2}$$

Finally, acute stress reduction of photosynthesis is further decomposed into reductions from soil water stress ($S_w$), temperature stress ($S_T$), and low humidity stress ($S_h$) as

$$\begin{aligned} S_w &= S_{\text{acute}}\left(P_{\text{pot}} - P_{ci}\right)\left(P_{\text{pot}} - P\right)^{-1} f_w(f_w + f_T)^{-1}, \\ S_T &= S_{\text{acute}}\left(P_{\text{pot}} - P_{ci}\right)\left(P_{\text{pot}} - P\right)^{-1} f_T(f_w + f_T)^{-1}, \\ S_h &= S_{\text{acute}}(P_{ci} - P)\left(P_{\text{pot}} - P\right)^{-1}, \end{aligned} \tag{C3}$$

where $f_x$ (subscript $T$ and $w$ for temperature and soil water) are an assimilation weighting of the $M_x$ stress factors of the general form

$$f_x = P_{\text{pot}}(1 - M_x)O_x, \tag{C4}$$

for which control coefficients ($O_x$) capture the degree to which the smoothed minimum of the three potential photosynthesis rates was influenced by the Rubisco- and PEP/sink-limited rates relevant for each type of stress (see Appendix A).

[40] Contributions to interannual variability are calculated with a similar procedure, but by replacing instantaneous (10-min) canopy-scale rates and stress scalars with their annual sums ($\Sigma_{ann}$) to partition the standard deviation (SD[.] operator below) of departure from a climatological annual, canopy-scale gross photosynthesis

$$\sigma_{tot} = \mathrm{SD}\left[\Sigma_{ann} P_{pot,climate} \Pi_{max} - \Sigma_{ann} P \Pi\right], \qquad (C5)$$

where a climatological potential is used because in this study we did not intend to address interannual fluctuations in potential photosynthesis. In this case of variability, proportional variance contributions are calculated from the variance (var[.] operator below) of annual reductions in photosynthesis due to acute stress or canopy radiation use ($X_{acute} = \mathrm{var}[1 - \Sigma_{ann} P / \Sigma_{ann} P_{pot,climate}]$ and $X_{veg} = \mathrm{var}[1 - \Sigma_{ann}\Pi / \Sigma_{ann}\Pi_{max}]$), as

$$K_{acute} = \frac{X_{acute}}{X_{acute} + X_{veg}}, \quad K_{veg} = \frac{X_{veg}}{X_{acute} + X_{veg}}. \qquad (C6)$$

Variability attributed to acute stress or canopy radiation use is

$$V_{acute} = K_{acute}\sigma_{tot}, \quad V_{veg} = K_{veg}\sigma_{tot}, \qquad (C7)$$

and variability from acute stress is further attributed as

$$\begin{aligned} V_w &= V_{acute}\mathrm{var}\left[\Sigma_{ann}\left\{\left(P_{pot,climate} - P_{ci}\right) f_w (f_w + f_T)^{-1}\right\}\right] \\ &\quad \cdot \mathrm{var}\left[\Sigma_{ann}\left(P_{pot,climate} - P\right)\right]^{-1}, \\ V_T &= V_{acute}\mathrm{var}\left[\Sigma_{ann}\left\{\left(P_{pot,climate} - P_{ci}\right) f_T (f_w + f_T)^{-1}\right\}\right] \\ &\quad \cdot \mathrm{var}\left[\Sigma_{ann}\left(P_{pot,climate} - P\right)\right]^{-1}, \\ V_h &= V_{acute}\mathrm{var}[\Sigma_{ann}(P_{ci} - P)]\mathrm{var}\left[\Sigma_{ann}\left(P_{pot,climate} - P\right)\right]^{-1}. \end{aligned} \qquad (C8)$$

Though complicated, this approach achieves an unambiguous quantification of the annual reduction due to each factor, or its interannual variability, with computational efficiency by avoiding the need for multiple simulations each calculating departure from a reference condition, as performed previously in a global application [*Schaefer et al.*, 2002].

[41] **Acknowledgments.** Funding for this study was provided by the United States National Aeronautics and Space Administration (NASA) Terrestrial Ecology Program (Diane Wickland) and the National Oceanic and Atmospheric Administration (NOAA) Global Carbon Cycle Program (Kathy Tedesco).

## References

Baker, D. F. (2007), Reassessing carbon sinks, *Science*, *316*(5832), 1708–1709, doi:10.1126/science.1144863.

Baker, D. F., et al. (2006), TransCom 3 inversion intercomparison: Impact of transport model errors on the interannual variability of regional $CO_2$ fluxes, 1988–2003, *Global Biogeochem. Cycles*, *20*, GB1002, doi:10.1029/2004GB002439.

Baker, I., A. S. Denning, N. Hanan, L. Prihodko, M. Uliasz, P.-L. Vidale, K. Davis, and P. Bakwin (2003), Simulated and observed fluxes of sensible and latent heat and $CO_2$ at the WLEF-TV tower using SiB2.5, *Global Change Biol.*, *9*, 1262–1277, doi:10.1046/j.1365-2486.2003.00671.x.

Ball, M. C., I. R. Cowan, and G. D. Farquhar (1988), Maintenance of leaf temperature and the optimization of carbon gain in relation to water-loss in a tropical mangrove forest, *Aust. J. Plant Physiol.*, *15*(1–2), 263–276.

Barr, A. G., T. A. Black, E. H. Hogg, T. J. Griffis, K. Morgenstern, N. Kljun, A. Theede, and Z. Nesic (2007), Climatic controls on the carbon and water balances of a boreal aspen forest, 1994–2003, *Global Change Biol.*, *13*(3), 561–576, doi:10.1111/j.1365-2486.2006.01220.x.

Bousquet, P., P. Peylin, P. Ciais, C. Le Quere, P. Friedlingstein, and P. P. Tans (2000), Regional changes in carbon dioxide fluxes of land and oceans since 1980, *Science*, *290*(5495), 1342–1346, doi:10.1126/science.290.5495.1342.

Cao, M. K., Q. F. Zhang, and H. H. Shugart (2001), Dynamic responses of African ecosystem carbon cycling to climate change, *Clim. Res.*, *17*, 183–193, doi:10.3354/cr017183.

Charney, J. G. (1975), The dynamics of deserts and droughts, *Q. J. R. Meteorol. Soc.*, *101*, 193–202, doi:10.1002/qj.49710142802.

Churkina, G., and S. W. Running (1998), Contrasting climatic controls on the estimated productivity of global terrestrial biomes, *Ecosystems*, *1*, 206–215, doi:10.1007/s100219900016.

Ciais, P., P. Friedlingstein, A. Friend, and D. S. Schimel (2001), Integrating global models of terrestrial primary productivity, in *Terrestrial Global Productivity*, edited by J. Roy, B. Saugier, and H. A. Mooney, pp. 449–478, Academic, San Diego.

Colello, G. D., C. Grivet, P. J. Sellers, and J. A. Berry (1998), Modeling of energy, water, and $CO_2$ flux in a temperate grassland ecosystem with SiB2: May–October 1987, *J. Atmos. Sci.*, *55*, 1141–1169, doi:10.1175/1520-0469(1998)055<1141:MOEWAC>2.0.CO;2.

Collatz, G. J., J. T. Ball, C. Grivet, and J. A. Berry (1991), Physiological and environmental regulation of stomatal conductance, photosynthesis and transpiration: A model that includes a laminar boundary layer, *Agric. For. Meteorol.*, *54*(2–4), 107–136, doi:10.1016/0168-1923(91)90002-8.

Collatz, G. J., M. Ribas-Carbo, and J. A. Berry (1992), Coupled photosynthesis-stomatal conductance model for leaves of $C_4$ plants, *Aust. J. Plant Physiol.*, *19*(5), 519–538.

Cramer, W., D. W. Kicklighter, A. Bondeau, B. Moore, C. Churkina, B. Nemry, A. Ruimy, and A. L. Schloss (1999), Comparing global models of terrestrial net primary productivity (NPP): Overview and key results, *Global Change Biol.*, *5*, 1–15, doi:10.1046/j.1365-2486.1999.00009.x.

Dai, Y. J., et al. (2003), The Common Land Model, *Bull. Am. Meteorol. Soc.*, *84*(8), 1013–1023.

DeFries, R. S., M. Hansen, J. R. G. Townshend, and R. Sohlberg (1998), Global land cover classifications at 8 km spatial resolution: The use of training data derived from Landsat imagery in decision tree classifiers, *Int. J. Remote Sens.*, *19*(16), 3141–3168, doi:10.1080/014311698214235.

Denning, A. S., G. J. Collatz, C. G. Zhang, D. A. Randall, J. A. Berry, P. J. Sellers, G. D. Colello, and D. A. Dazlich (1996), Simulations of terrestrial carbon metabolism and atmospheric $CO_2$ in a general circulation model. Part 1. Surface carbon fluxes, *Tellus Ser. B*, *48*(4), 521–542, doi:10.1034/j.1600-0889.1996.t01-2-00009.x.

Denning, A. S., M. E. Nicholls, L. Prihodko, P.-L. Vidale, I. Baker, K. Davis, and P. Bakwin (2003), Simulated and observed variations in atmospheric carbon dioxide over a Wisconsin forest using a coupled ecosystem-atmosphere model, *Global Change Biol.*, *9*, 1241–1250, doi:10.1046/j.1365-2486.2003.00613.x.

Farquhar, G. D., S. V. Caemmerer, and J. A. Berry (1980), A biochemical-model of photosynthetic $CO_2$ assimilation in leaves of $C_3$ species, *Planta*, *149*(1), 78–90, doi:10.1007/BF00386231.

Hanan, N. P., J. A. Berry, S. B. Verma, E. A. Walter-Shea, A. E. Suyker, G. G. Burba, and A. S. Denning (2005), Testing a model of $CO_2$, water and energy exchange in Great Plains tallgrass prairie and wheat ecosystems, *Agric. For. Meteorol.*, *131*(3–4), 162–179, doi:10.1016/j.agrformet.2005.05.009.

Hansen, M. C., R. S. Defries, J. R. G. Townshend, and R. Sohlberg (2000), Global land cover classification at 1 km spatial resolution using a classification tree approach, *Int. J. Remote Sens.*, *21*(6–7), 1331–1364, doi:10.1080/014311600210209.

Herrmann, S. M., A. Anyamba, and C. J. Tucker (2005), Recent trends in vegetation dynamics in the African Sahel and their relationship to climate, *Glob. Environ. Change*, *15*, 394–404, doi:10.1016/j.gloenvcha.2005.08.004.

Houghton, R. A. (2000), Interannual variability in the global carbon cycle, *J. Geophys. Res.*, *105*(D15), 20,121–20,130, doi:10.1029/2000JD900041.

Imhoff, M. L., L. Bounoua, T. Ricketts, C. Loucks, R. Harriss, and W. T. Lawrence (2004), Global patterns in human consumption of net primary production, *Nature*, *429*, 870–873, doi:10.1038/nature02619.

Intergovernmental Panel on Climate Change (2001), *Climate Change 2001: Synthesis Report, Third Assessment Report of the Intergovernmental Panel on Climate Change*, Cambridge Univ. Press, New York.

Knapp, A. K., and M. D. Smith (2001), Variation among biomes in temporal dynamics of aboveground primary production, *Science*, *291*, 481–484.

Los, S. O. (1998), Linkages between global vegetation and climate: An analysis based on NOAA-Advanced Very High Resolution Radiometer Data, Ph.D. dissertation, Vrije Universiteit, Amsterdam.

Los, S. O., G. J. Collatz, P. J. Sellers, C. M. Malmstrom, N. H. Pollack, R. S. DeFries, L. Bounoua, M. T. Parris, C. J. Tucker, and D. A. Dazlich (2000), A global 9-yr biophysical land surface dataset from NOAA AVHRR data, *J. Hydrometeorol.*, *1*(2), 183–199, doi:10.1175/1525-7541(2000)001<0183:AGYBLS>2.0.CO;2.

McGuire, A. D., et al. (2001), Carbon balance of the terrestrial biosphere in the twentieth century: Analyses of $CO_2$, climate and land use effects with four process-based ecosystem models, *Global Biogeochem. Cycles*, *15*(1), 183–206, doi:10.1029/2000GB001298.

Mitchell, T. D., and P. D. Jones (2005), An improved method of constructing a database of monthly climate observations and associated high-resolution grids, *Int. J. Climatol.*, *25*(6), 693–712, doi:10.1002/joc.1181.

Nemani, R. R., C. D. Keeling, H. Hashimoto, W. M. Jolly, S. C. Piper, C. J. Tucker, R. B. Myneni, and S. W. Running (2003), Climate-driven increases in global terrestrial net primary production from 1982 to 1999, *Science*, *300*(5625), 1560–1563, doi:10.1126/science.1082750.

New, M., M. Hulme, and P. Jones (2000), Representing twentieth-century space-time climate variability. Part II: Development of 1901–96 monthly grids of terrestrial surface climate, *J. Clim.*, *13*(13), 2217–2238, doi:10.1175/1520-0442(2000)013<2217:RTCSTC>2.0.CO;2.

Nicholson, S. E. (2000), The nature of rainfall variability over Africa on time scales of decades to millenia, *Global Planet. Change*, *26*(1–3), 137–158, doi:10.1016/S0921-8181(00)00040-0.

Nicholson, S. E., and D. Entekhabi (1986), The quasi-periodic behavior of rainfall variability in Africa and its relationship to the Southern Oscillation, *Meteorol. Atmos. Phys.*, *34*(3–4), 311–348.

Nicholson, S. E., C. J. Tucker, and M. B. Ba (1998), Desertification, drought, and surface vegetation: An example from the West African Sahel, *Bull. Am. Meteorol. Soc.*, *79*, 815–829, doi:10.1175/1520-0477(1998)079<0815:DDASVA>2.0.CO;2.

Olsson, L., L. Eklundh, and J. Ardö (2005), A recent greening of the Sahel-trends, patterns and potential causes, *J. Arid Environ.*, *63*, 556–566, doi:10.1016/j.jaridenv.2005.03.008.

Pinzon, J. (2002), Using HHT to successfully uncouple seasonal and interannual components in remotely sensed data, paper presented at SCI 2002 Conference, Long-Term Ecol. Res. Network, Orlando, Florida, 14–18 July.

Pinzon, J., M. E. Brown, and C. J. Tucker (2005), Satellite time series correction of orbital drift artifacts using empirical mode decomposition, in *Hilbert-Huang Transform: Introduction and Applications*, edited by N. Huang and S. S. P. Shen, pp. 167–186, World Sci., Hackensack, N. J.

Potter, C. S. (1999), Terrestrial biomass and the effects of deforestation on the global carbon cycle: Results from a model of primary production using satellite observations, *BioScience*, *49*, 769–778, doi:10.2307/1313568.

Potter, C. S., S. Klooster, R. Myneni, V. Genovese, P. N. Tan, and V. Kumar (2003), Continental-scale comparisons of terrestrial carbon sinks estimated from satellite data and ecosystem modeling 1982–1998, *Global Planet. Change*, *39*, 201–213, doi:10.1016/j.gloplacha.2003.07.001.

Prince, S. D., E. Brown de Colstoun, and L. Kravitz (1998), Evidence from rain use efficiencies does not support extensive Sahelian desertification, *Global Change Biol.*, *4*, 359–374, doi:10.1046/j.1365-2486.1998.00158.x.

Prince, S. D., K. J. Wessels, C. J. Tucker, and S. E. Nicholson (2007), Desertification in the Sahel: A reinterpretation of a reinterpretation, *Global Change Biol.*, *13*, 1308–1313, doi:10.1111/j.1365-2486.2007.01356.x.

Rayner, P. J., M. Scholze, W. Knorr, T. Kaminski, R. Giering, and H. Widmann (2005), Two decades of terrestrial carbon fluxes from a carbon cycle data assimilation system (CCDAS), *Global Biogeochem. Cycles*, *19*, GB2026, doi:10.1029/2004GB002254.

Reichstein, M., et al. (2007), Reduction of ecosystem productivity and respiration during the European summer 2003 climate anomaly: A joint flux tower, remote sensing and modelling analysis, *Global Change Biol.*, *13*(3), 634–651, doi:10.1111/j.1365-2486.2006.01224.x.

Rödenbeck, C., S. Houweling, M. Gloor, and M. Heimann (2003), $CO_2$ flux history 1982–2001 inferred from atmospheric data using a global inversion of atmospheric transport, *Atmos. Chem. Phys.*, *3*, 1919–1964.

Schaefer, K., A. S. Denning, N. Suits, J. Kaduk, I. Baker, S. Los, and L. Prihodko (2002), Effect of climate on interannual variability of terrestrial $CO_2$ fluxes, *Global Biogeochem. Cycles*, *16*(4), 1102, doi:10.1029/2002GB001928.

Schaefer, K., G. J. Collatz, P. Tans, A. S. Denning, I. Baker, J. Berry, L. Prihodko, N. Suits, and A. Philpott (2008), Combined Simple Biosphere/Carnegie-Ames-Stanford Approach terrestrial carbon cycle model, *J. Geophys. Res.*, *113*, G03034, doi:10.1029/2007JG000603.

Sellers, P. J., Y. Mintz, Y. C. Sud, and A. Dalcher (1986), The design of a simple biosphere model (SiB) for use within general circulation models, *J. Atmos. Sci.*, *43*, 505–531, doi:10.1175/1520-0469(1986)043<0505:ASBMFU>2.0.CO;2.

Sellers, P. J., J. A. Berry, G. J. Collatz, C. B. Field, and F. G. Hall (1992), Canopy reflectance, photosynthesis, and transpiration. Part 3. A reanalysis using improved leaf models and a new canopy integration scheme, *Remote Sens. Environ.*, *42*(3), 187–216, doi:10.1016/0034-4257(92)90102-P.

Sellers, P. J., C. J. Tucker, G. J. Collatz, S. O. Los, C. O. Justice, D. A. Dazlich, and D. A. Randall (1994), A global 1° by 1° NDVI data set for climate studies. Part 2. The generation of global fields of terrestrial biophysical parameters from the NDVI, *Int. J. Remote Sens.*, *15*(17), 3519–3545, doi:10.1080/01431169408954343.

Sellers, P. J., et al. (1996a), Comparison of radiative and physiological effects of doubled atmospheric $CO_2$ on climate, *Science*, *271*(5254), 1402–1406, doi:10.1126/science.271.5254.1402.

Sellers, P. J., S. O. Los, C. J. Tucker, C. O. Justice, D. A. Dazlich, G. J. Collatz, and D. A. Randall (1996b), A revised land surface parameterization (SiB2) for atmospheric GCMs. Part 2. The generation of global fields of terrestrial biophysical parameters from satellite data, *J. Clim.*, *9*(4), 706–737, doi:10.1175/1520-0442(1996)009<0706:ARLSPF>2.0.CO;2.

Sellers, P. J., D. A. Randall, G. J. Collatz, J. A. Berry, C. B. Field, D. A. Dazlich, C. Zhang, G. D. Collelo, and L. Bounoua (1996c), A revised land surface parameterization (SiB2) for atmospheric GCMs. Part 1. Model formulation, *J. Clim.*, *9*(4), 676–705, doi:10.1175/1520-0442(1996)009<0676:ARLSPF>2.0.CO;2.

Still, C. J., J. A. Berry, G. J. Collatz, and R. S. DeFries (2003), Global distribution of $C_3$ and $C_4$ vegetation: Carbon cycle implications, *Global Biogeochem. Cycles*, *17*(1), 1006, doi:10.1029/2001GB001807.

Tempel, P., N. H. Batjes, and V. W. P. van Engelen (1996), IGBP-DIS soil data set for pedotransfer function development, *Working Pap. Preprint 96/05*, Int. Soil Ref. and Inf. Cent., Wageningen, Netherlands.

Tucker, C. J., J. E. Pinzon, M. E. Brown, D. Slayback, E. W. Pak, R. Mahoney, E. Vermote, and N. El Saleous (2006), An extended AVHRR 8-km NDVI dataset compatible with MODIS and SPOT vegetation NDVI data, *Int. J. Remote Sens.*, *26*, 4485–4498.

Tyson, P. D., G. R. J. Cooper, and T. S. McCarthy (2002), Millennial to multi-decadal variability in the climate of southern Africa, *Int. J. Climatol.*, *22*(9), 1105–1117, doi:10.1002/joc.787.

van der Werf, G. R., J. T. Randerson, L. Giglio, G. J. Collatz, P. S. Kasibhatla, and A. F. Arellano (2006), Interannual variability in global biomass burning emissions from 1997 to 2004, *Atmos. Chem. Phys.*, *6*, 3423–3441.

Verma, S. B., J. Kim, and R. J. Clement (1992), Momentum, water vapor, and carbon dioxide exchange at a centrally located prairie site during FIFE, *J. Geophys. Res.*, *97*(D17), 18,629–18,639.

Vidale, P. L., and R. Stöckli (2005), Prognostic canopy air space solutions for land surface exchanges, *Theor. Appl. Climatol.*, *80*, 245–257, doi:10.1007/s00704-004-0103-2.

Williams, C. A., N. P. Hanan, J. C. Neff, R. J. Scholes, J. A. Berry, A. S. Denning, and D. F. Baker (2007), Africa and the global carbon cycle, *Carbon Balance Manag.*, *2*, 1–13, doi:10.1186/1750-0680-2-3.

Woodrow, I. E., and J. A. Berry (1988), Enzymatic regulation of photosynthetic $CO_2$ fixation in $C_3$ plants, *Annu. Rev. Plant Physiol.*, *39*, 533–594.

I. Baker and A. S. Denning, Department of Atmospheric Sciences, Colorado State University, Fort Collins, CO 80523-1371, USA.

J. Berry, Carnegie Institution of Washington, 1530 P Street NW, Washington, DC 20005, USA.

G. J. Collatz, Biospheric Sciences Branch, Hydrospheric and Biospheric Sciences Laboratory, NASA Goddard Space Flight Center, Code 614.4, Greenbelt, MD 20771, USA.

N. P. Hanan, Natural Resource Ecology Laboratory, Colorado State University, Fort Collins, CO 80523-1499, USA.

C. A. Williams, Graduate School of Geography, Clark University, 950 Main Street, Worcester, MA 01610, USA. (cwilliams@clarku.edu)